

Dynamics of edge currents in a linearly quenched Haldane model

Sougata Mardanya, Utso Bhattacharya, Amit Agarwal,^{*} and Amit Dutta[†]
Department of Physics, Indian Institute of Technology, Kanpur, Kanpur 208016, India

 (Received 28 January 2018; revised manuscript received 12 March 2018; published 26 March 2018)

In a finite-time quantum quench of the Haldane model, the Chern number determining the topology of the bulk remains invariant, as long as the dynamics is unitary. Nonetheless, the corresponding boundary attribute, the edge current, displays interesting dynamics. For the case of sudden and adiabatic quenches the postquench edge current is solely determined by the initial and the final Hamiltonians, respectively. However for a finite-time (τ) linear quench in a Haldane nanoribbon, we show that the evolution of the edge current from the sudden to the adiabatic limit is not monotonic in τ and has a turning point at a characteristic time scale $\tau = \tau_0$. For small τ , the excited states lead to a huge unidirectional surge in the edge current of both edges. On the other hand, in the limit of large τ , the edge current saturates to its expected equilibrium ground-state value. This competition between the two limits lead to the observed nonmonotonic behavior. Interestingly, τ_0 seems to depend only on the Semenoff mass and the Haldane flux. A similar dynamics for the edge current is also expected in other systems with topological phases.

DOI: [10.1103/PhysRevB.97.115443](https://doi.org/10.1103/PhysRevB.97.115443)

I. INTRODUCTION

Subtle topological phenomena such as the imaging of edge states in cold-atomic quantum Hall systems [1] and the direct measurement of the Berry curvature [2] and the Zak phase [3] have been demonstrated in cold-atomic topological bands. Beyond these static situations, the dynamical topological properties of systems following a quantum quench have also been experimentally probed [4–6]. A quantum quench forces the initial state prepared in the quantum many-body ground state of the initial Hamiltonian to undergo dynamical evolution far from equilibrium [7]. Thus quantum quenches offer the promise of engineering distinct many-body nonequilibrium states which have no equilibrium counterpart [8–13]. This has motivated a plethora of studies of the nonequilibrium dynamics of both closed and open topological quantum systems under the application of quantum quenches [14–33] and periodic drives [34–47].

More recently there has been significant interest in the dynamics of the edge current following a quantum quench in a system, taking it either from a topological phase to a trivial insulator phase or vice versa. The possibility of measuring the static topological index through a dynamical quench has also been explored [48,49]. Studying the Haldane model [50], Cao *et al.* [51] showed that the Chern number of the initial phase in the translationally invariant Haldane model remains preserved throughout the postquench unitary evolution of the system, irrespective of the topology of the final Hamiltonian (see also [52]). The invariance of the Chern number under any unitary dynamics has also been rigorously established by Alessio *et al.* [53]. The invariance of the Chern number has also been shown for the quantum quench in the Haldane model with higher order

hoppings [54,55]. The preservation of the winding number of the many-body state was also mentioned [56,57] in the context of quenches in interacting topological BCS superfluids. However, the dynamics of the edge current following quench in these systems and the fate of the corresponding ‘bulk-boundary correspondence’ still remains an interesting open question following general forms of quench. Motivated by this, in this article we study the dynamics of the edge current in a *finite-time linear quench* across the topological phase transition point, by varying the Semenoff mass in a Haldane nanoribbon.

Earlier studies on the Haldane model [51], and the Haldane model with higher hopping [54], showed that following a global *sudden* quench from a topological to a nontopological phase, the edge current relaxes from a finite value to a postquench value close to 0—which is the value corresponding to the ground state of the final Hamiltonian. In this article we focus on the role of the finite rate of the quench on the dynamics of the edge current, by considering a linear finite-time quenching of the Semenoff mass [58] in the Haldane nanoribbon [50], taking it from a trivial to a topological phase. Interestingly, we show that in quenching from the nontopological phase to the topological phase, the edge current evolves in a nonmonotonic way as a function of the quenching rate (τ) and has a turning point when τ is increased from the sudden ($\tau = 0$) to the adiabatic ($\tau \rightarrow \infty$) limit.

The paper is organized as follows: The equilibrium Haldane model is introduced in Sec. II, which also discusses the equilibrium edge current for the model in a nanoribbon geometry, periodically wrapped in the x direction and open in the y direction. This is followed by a discussion of the impact of a sudden and adiabatic quench, driving the system from the nontopological phase to the topological phase, on the edge current in Sec. III. The role of a finite-time linear quench in the dynamics of the edge current is described in Sec. IV. Finally, we summarize our findings in Sec. V.

^{*}amitag@iitk.ac.in

[†]dutta@iitk.ac.in

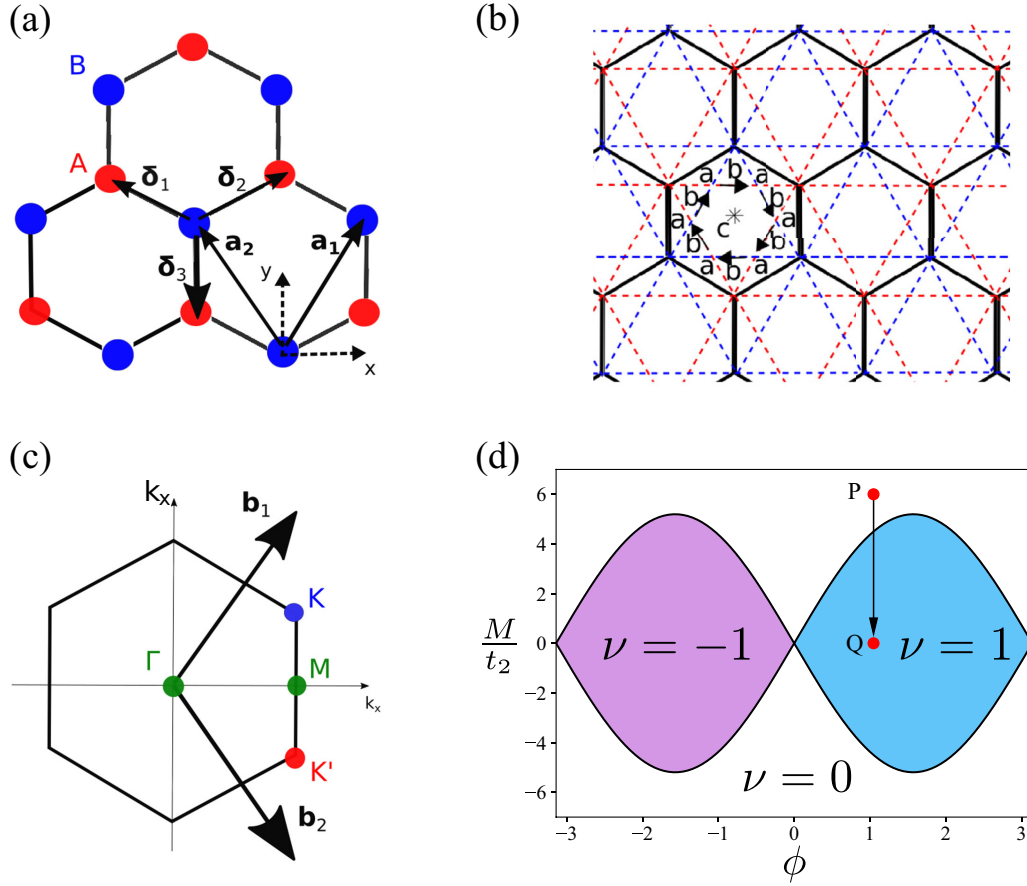


FIG. 1. (a) Three plaquettes of the hexagonal lattice with lattice vectors \mathbf{a}_1 and \mathbf{a}_2 . Blue and red circles represent the two sublattices A and B. (b) The Haldane lattice, with locally broken time-reversal symmetry. Regions labeled “a” and “b” enclose flux in opposite directions, and arrows on the next-nearest bonds (dashed lines) denote the direction of positive phase hopping due to the locally broken time-reversal invariance. (c) Brillouin zone of a hexagonal lattice with reciprocal lattice vectors \mathbf{b}_1 and \mathbf{b}_2 , with \mathbf{K} and \mathbf{K}' representing the two inequivalent Dirac points; the color corresponds to sublattices A and B. (d) Chern phase diagram of the Haldane model in the on-site energy, M (also called the Semenoff mass), and the staggered phase, ϕ , plane. The white region is the topologically trivial phase ($\nu = 0$), while the colored region is the topologically nontrivial Chern phase ($\nu = \pm 1$). The arrow indicates a quenching scheme of varying M , which takes the model from point P ($\phi = \pi/3$, $M/t_2 = 6$) in the nontopological phase to point Q ($\phi = \pi/3$, $M/t_2 = 0$) in the topological phase.

II. THE HALDANE MODEL

Our starting point is the Haldane model with broken spatial inversion and locally broken time-reversal symmetry, describing the nearest and next-nearest hopping of spinless electrons on a hexagonal lattice. The two-dimensional (2D) hexagonal graphenelike lattice composed of the two triangular sublattices A and B is shown in Fig. 1(a). The Hamiltonian of this model is explicitly given by

$$H = \sum_{\langle i,j \rangle} t_1 (c_{iA}^\dagger c_{jB} + \text{H.c.}) + M \sum_{i \in A} \hat{n}_i - M \sum_{i \in B} \hat{n}_i + \sum_{\langle\langle i,j \rangle\rangle} t_2 e^{i\phi_{ij}} (c_{iA}^\dagger c_{jA} + c_{iB}^\dagger c_{jB} + \text{H.c.}), \quad (1)$$

where c_i^\dagger (c_i) is the fermionic creation (annihilation) operator at site i satisfying the anticommutation relation $\{c_i^\dagger, c_j\} = \delta_{ij}$. In Eq. (1), $\hat{n}_i = c_i^\dagger c_i$ and A and B denote the two sublattices. The phase factor, $\phi_{ij} = \pm\phi$, is positive for counterclockwise hopping and negative for clockwise hopping. It mimics a

staggered magnetic field, introduced to break the local time-reversal symmetry. Note that the total net magnetic flux through each hexagonal plaquette is 0, conserving the global time-reversal symmetry. This staggered magnetic field, breaking the local time-reversal symmetry is what renders the model topologically nontrivial. On the other hand, the different Semenoff mass terms M ($-M$) for the two sublattices, A (B), break the spatial inversion symmetry of the model.

The real-space tight-binding Hamiltonian of Eq. (1) with periodic boundary conditions in both directions can also be expressed in the crystal-momentum space via a Fourier transform and is given by

$$H = \begin{pmatrix} c_{kA}^\dagger & c_{kB}^\dagger \end{pmatrix} h(\mathbf{k}) \begin{pmatrix} c_{kA} \\ c_{kB} \end{pmatrix}, \quad \text{where } h(\mathbf{k}) = \sum_{i=0}^3 h_i(\mathbf{k}) \sigma_i. \quad (2)$$

Here σ_i (for $i = 1, 2, 3$) are the three Pauli spin matrices, and σ_0 is the 2×2 identity matrix. The components $h_i(\mathbf{k})$ are

$$h_0(\mathbf{k}) = 2t_1 \cos \phi [\mathbf{k} \cdot \cos(\mathbf{k} \cdot \mathbf{a}_1) + \cos(\mathbf{k} \cdot \mathbf{a}_2) + \cos(\mathbf{k} \cdot (\mathbf{a}_1 - \mathbf{a}_2))],$$

$$\begin{aligned}
h_1(\mathbf{k}) &= t_1[1 + \cos(\mathbf{k}\cdot\mathbf{a}_1) + \cos(\mathbf{k}\cdot\mathbf{a}_2)], \\
h_2(\mathbf{k}) &= t_1[\sin(\mathbf{k}\cdot\mathbf{a}_1) + \sin(\mathbf{k}\cdot\mathbf{a}_2)], \\
h_3(\mathbf{k}) &= M + M_H, \\
M_H(\mathbf{k}) &= 2t_2 \sin \phi [\sin(\mathbf{k}\cdot\mathbf{a}_2) - \sin(\mathbf{k}\cdot\mathbf{a}_1) \\
&\quad + \sin(\mathbf{k}\cdot(\mathbf{a}_1 - \mathbf{a}_2))]. \tag{3}
\end{aligned}$$

Here $M_H(\mathbf{k})$ is the staggered field and crystal-momentum-dependent Haldane mass and $\mathbf{a}_1 = \frac{a}{2}(\sqrt{3}, 3)$, $\mathbf{a}_2 = \frac{a}{2}(-\sqrt{3}, 3)$ as shown in Fig. 1(a). For $M = 0$ and $\phi = 0$ the Hamiltonian in Eq. (1) reduces to the second nearest-neighbor tight-binding Hamiltonian of graphene, which has a Dirac-like dispersion at six points in the hexagonal Brillouin zone, with only two of them being inequivalent. These two inequivalent points are time-reversed partners of each other [see Fig. 1(c)]. The other Dirac points are related to these two via reciprocal lattice vectors.

Qualitatively, when the local time-reversal symmetry-breaking term (ϕ) dominates over the inversion symmetry-breaking term (M) in the translationally invariant Haldane model, it is topologically characterized by a bulk Chern number which takes the value $\nu = \pm 1$ and 0 otherwise. The Chern phase diagram of the Haldane model is shown in Fig. 1(d). When the Chern number of the bulk system is ± 1 , the boundary of the finite-sized open system hosts charge-conducting edge modes, consistent with the bulk-boundary correspondence.

Edge current

To explore the dynamical evolution of the edge current following a quench, we consider the edge states of the Haldane model, which is periodic (and thus translationally invariant) in the x direction and has finite width N along the y direction with an armchair edge. The schematic for the same is depicted in Fig. 2. Using the conserved crystal momentum along the periodic x direction, while retaining the real-space description in the y direction, we obtain the Hamiltonian

$$\begin{aligned}
H &= \sum_{k_x} \sum_{m,n=1}^L \sum_{m',n'=n-1}^{n+1} \sum_{s=A,B} e^{ik_x x_{mns}} c_{k_x,ns}^\dagger \\
&\quad \times \{ \delta_{m,m'} \delta_{n,n'} M_s c_{k_x,n\bar{s}} e^{-ik_x x_{mns}} + t_1 c_{k_x,n'\bar{s}} e^{-ik_x x_{m'n's}} \\
&\quad + t_2 e^{i\phi_{mm'/nn'}} c_{k_x,n'\bar{s}} e^{-ik_x x_{m'n's}} \}, \tag{4}
\end{aligned}$$

where $\bar{s} \neq s$, and $M_s = +M$ ($-M$) for $s = A$ ($s = B$).

The energy spectrum of this semiopen model for both the topological and the trivial phase is shown in Fig. 3. To clearly exhibit a correspondence between the bulk Chern number (in a periodically wrapped system along both directions) and the number of midgap band crossings in the semiopen system, we choose two sets of parameter values corresponding to the two phases in the phase diagram in Fig. 1(d) with $\nu = 0$ and -1 . In the nontopological phase, i.e., for $\nu = 0$, there are no band crossings in the spectrum [see Fig. 3(a)], indicating the absence of conducting edge states. On the other hand, when we are in the topologically nontrivial phase with Chern number $\nu = -1$, the spectrum in Fig. 3(b) clearly shows a midgap band crossing between the valance band and the conduction band at $k_x = 0$.

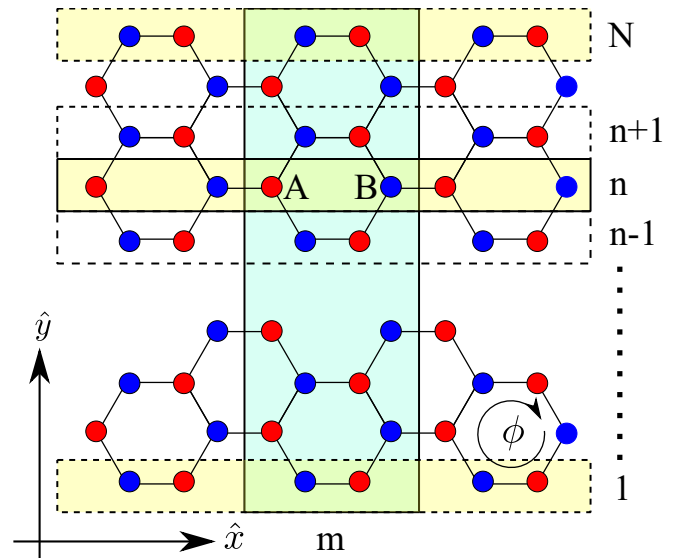


FIG. 2. Haldane model on a nanoribbon, which is periodic along the armchair edge (x direction) and finite along the zigzag direction (y direction). The nanoribbon is N cells wide and each unit cell is labeled with two indices, m and n , and has two lattice sites (A or B). The phase of the complex hopping t_2 is negative (positive) for hopping in a clockwise (counterclockwise) sense between next-nearest neighbors.

The local current operator at any site i is given by

$$\hat{J}_i = -\frac{i}{2} \sum_j \vec{\delta}_{ij} (t_{ij} c_i^\dagger c_j - \text{H.c.}), \tag{5}$$

where t_{ij} and $\vec{\delta}_{ij}$ are the hopping amplitude and vector displacement between site i and site j , respectively. The sum involving index j is over the nearest and next-nearest-neighbor sites to i only. Each site of this ribbon is labeled $\{m, n, s\}$, where $\{m, n\}$ denotes the position of the site in the 2D lattice and s is the sublattice index (A or B) of that site. The total current flowing along the strip in the x direction for a particular value of n (where n labels each horizontal row along the y direction; see Fig. 2) is obtained from the relation

$$J_n^x = \langle \hat{J}_n^x \rangle = \sum_{k_x, s} \langle \hat{J}_{n, k_x, s}^x \rangle,$$

where the expectation is taken over the ground state of the Hamiltonian under equilibrium conditions and over the dynamically evolved ground state of the system in the case of a quenched system [55].

Figure 4 shows the average equilibrium current in the x direction plotted versus $n = 1, \dots, N$ when the system is in the $\nu = 1$ phase ($M = 0$ and $\phi = \pi/3$). As expected, there are two counter-propagating channels of current near the system edges (at $n = 1$ and N), while the current in the bulk is 0 throughout. Moreover, the equilibrium current for the topologically trivial gapped phase with $\nu = 0$ is identically 0 throughout the system.

III. EDGE CURRENT DYNAMICS FOLLOWING SUDDEN AND ADIABATIC QUANTUM QUENCH

In order to investigate the nonequilibrium dynamics of the edge current of the Haldane model, we consider quantum

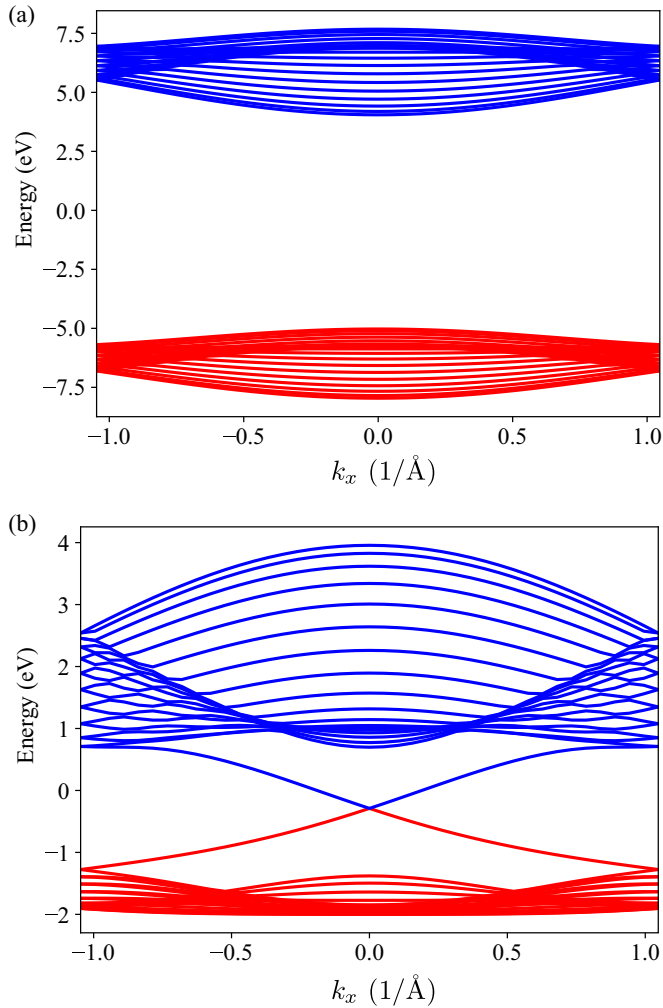


FIG. 3. Energy spectrum of the Haldane nanoribbon described by the Hamiltonian in Eq. (4) in (a) the topologically trivial phase with $M = 6$ and Chern number $\nu = 0$ and (b) the topological phase with $M = 0$ and $\nu = -1$. Blue and red lines represent the conduction and the valance bands, respectively. Note that unlike the topologically trivial phase, the topological phase has a single band crossing at $k_x = 0$. We have chosen other parameters to be $t_1 = 1$, $t_2 = 1/3$, $\phi = \pi/3$, and $N = 20$.

quenches between different points (M, ϕ) of the phase diagram shown in Fig. 1(d). The values of the hopping amplitude t_1 and t_2 are kept fixed, and we look at the edge current at the N th row of the sample. A relevant question to ask here is whether we should look at only the edge row or at a few rows subsequent to the end rows, as the edge states at the end rows have a localization length that falls off inwards from the boundary of the sample. We note that Fig. 4 shows a special scenario used in our work, to enable easy comparison with the sudden quench scenario as performed by Cao *et al.* But as such, tweaking the second-nearest-neighbor interactions by tuning t_2 and ϕ , we can easily observe that the current at the first and the last rows of the lattice are maximum and they fall off exponentially moving away from the edge. This is a common scenario encountered by varying t_2 and ϕ across most of the phase diagram. Thus, in this scenario even if we consider other sites within the localization length of the edge states other than just the last row at the

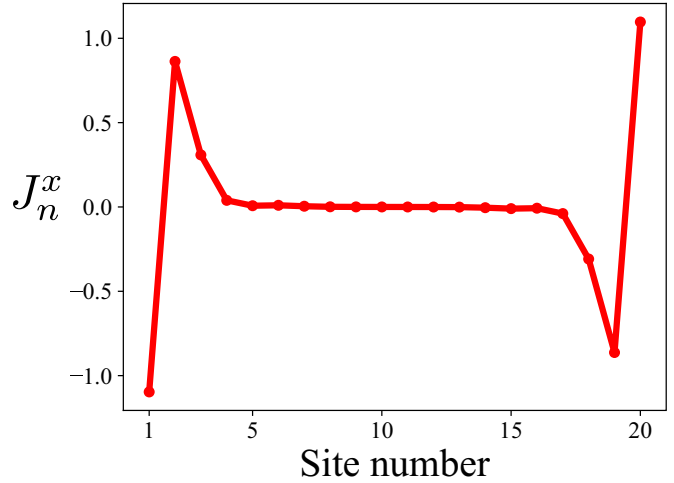


FIG. 4. Average equilibrium current in the x direction along each row, $n = 1, \dots, 20$, of the Haldane nanoribbon (see Fig. 2) in the topological phase. Two counter-propagating current-carrying states appear at the two edges. On the other hand, the current remains 0 in the bulk. Here we have chosen $t_1 = 1$, $t_2 = 1/3$, $M = 0$, $\phi = \pi/3$, and $N = 20$. (See also Fig. 4(a) of Cao *et al.* [51].)

boundary, our conclusions about the dynamics of the edge current would remain the same. Therefore, we calculate the current at the end strips only to cover all such situations in general. To start with, at time $t = 0$, the system is initially in its ground state with parameter (M_i, ϕ_i) . At half-filling the initial state of the system occupies the valence band completely. The system is now driven to a different phase by either changing a parameter abruptly or through a linear time-dependent sweep from (M_i, ϕ_i) to a new set of values (M_f, ϕ_f) . The system then unitarily evolves under the action of the new Hamiltonian, $H(M_f, \phi_f)$.

Earlier studies [51,53] established that the Chern number of the initial ground state of the translationally invariant Haldane model remains preserved throughout the postquench unitary evolution for all possible quenching protocols. However, the preservation of the bulk topological invariant (Chern number) is not reflected in the dynamics of the boundary (edge) current. Following a sudden quench, the edge current was shown to attain a new equilibrium value close to the ground-state expectation value of the edge current evaluated for the final Hamiltonian.

Motivated by this, we investigate the time evolution of the edge current for a Haldane model on a nanoribbon geometry subjected to a slow quench, a linear time-dependent sweep, from one phase to the other. To this end, we start with the system in the ground state of the initial Hamiltonian with parameter (M_i, ϕ_i) . Now the Semenoff mass $M(t)$ is changed linearly with time over a given interval, keeping ϕ fixed, such that the final state is specified by point $(M_f, \phi_f = \phi_i)$ in the phase diagram in Fig. 1(d). Explicitly, the quench protocol is given by $M(t) = M_i + (M_f - M_i)t/\tau$ for times $0 \leq t \leq \tau$, where $1/\tau$ specifies the rate of the ramp.

We note that the problem is analytically intractable for the following complications: for a nanoribbonlike geometry the system can be viewed as a finite-time multilevel Landau-Zener

problem with $2N$ number of levels. For infinite time duration [59,60], this problem can only be solved by using independent level (IL) approximation as illustrated by Shytov *et al.* [61]. However, the finite-duration dynamics considered in this work is immensely complicated even for the two-level Landau-Zener problem [62,63]. Additionally, the IL approximation has the following shortcomings: (i) the IL approximation does not necessarily hold true, and (ii) the IL approximation results in loss of phase coherence, which needs to be retained to probe the topology, as done in this paper. We therefore resort to numerical methods to calculate the final edge current by taking the expectation value of the current operator in Eq. (5) along the x direction. The expectation value is calculated with respect to the time-evolved initial state of the system obtained after solving the $2N$ coupled linear time-dependent equations for every value of k_x , keeping M_i, M_f , and ϕ fixed throughout (see the Appendix for further details). The time evolution of the edge current, when we sweep our system ($L = 20$) from nontopological ($M = 6, \phi = \pi/3$) to topological ($M = 0, \phi = \pi/3$) phase followed by a unitary evolution, is shown in Fig. 5. Here the edge current is shown for the $n = 20$ edge, and the current at the opposite edge ($n = 1$) is of the same magnitude but flows in the opposite direction. For the particular case $\tau \rightarrow 0$, we are in the sudden quench regime, and for $\tau \rightarrow \infty$, the quench is adiabatic.

A. Sudden quench limit

In Figs. 5(a) and 5(b), initially the system is in a nontopological phase, and consequently the edge current always starts from its equilibrium value of 0. For the case of sudden quench, $\tau = 0$, the system remains ‘frozen’ in the initial state, i.e., the ground state of the system in the nontopological phase, and thus the current following a sudden quench is 0 when measured immediately after the quench. However, the edge current has a nontrivial dynamics if the system is allowed to evolve with the final Hamiltonian [51]. Nonetheless, Fig. 5(a) shows a small but finite value of the postquench current. In the case of small τ , the system gets excited to higher energy states as well, all of which eventually do a free evolution with the final Hamiltonian. Thus the edge current is primarily governed by the overlap between the initial ground state and the eigenstates of the final Hamiltonian [see Fig. 5(a)]. The oscillations in the edge current are shown in Fig. 5(a).

B. Adiabatic quench

The opposite limit of the adiabatic quench can be understood by employing the Landau-Zener argument for two midgap states. For no diabatic transitions (mixing of energy levels) we have $\tau \gg 1/\Delta^2$, where Δ is the equilibrium gap in the spectrum for the first excited state. Now since the energy gap in our system scales inversely with L , we have $\tau > L^2$ for an adiabatic evolution of the system—in which the system state follows the instantaneous ground state of the time-evolved Hamiltonian at all times. Thus for a system size of $L = 20$, the adiabatic limit is achieved for a value of $\tau > 400$. Consequently, in Fig. 5(b), we see that the current reaches a finite value infinitesimally close to the equilibrium current of the final Hamiltonian with $M = M_f$ and $\phi = \phi_f$, as expected.

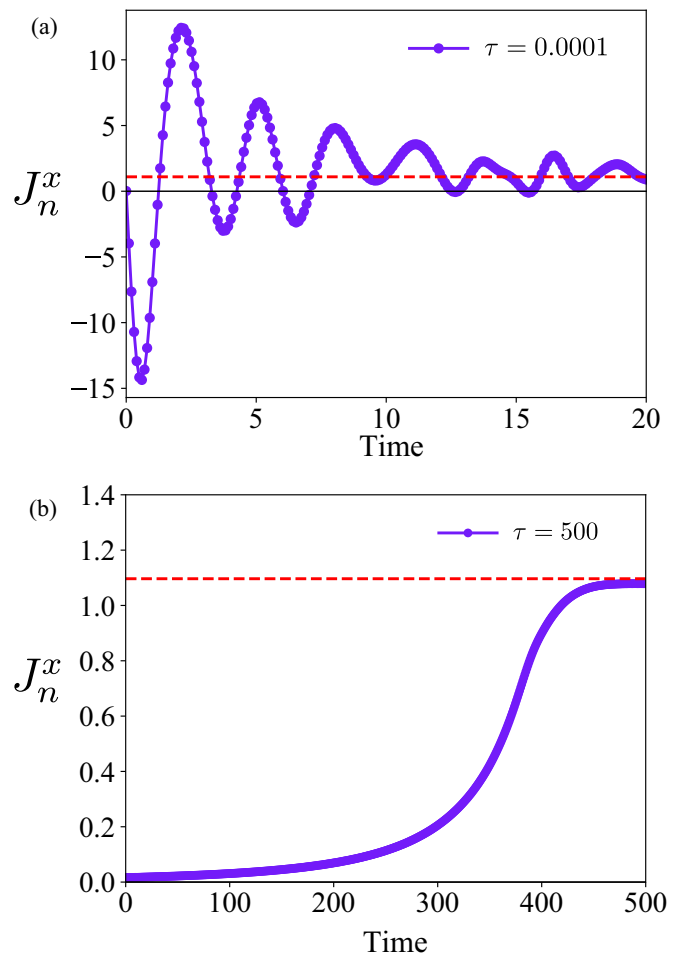


FIG. 5. Dynamics of the edge current from the nontopological phase ($M = 6, \phi = \pi/3$) to the topological phase ($M = 0, \phi = \pi/3$) following two quenching protocols. (a) A sudden quench, when the rate of quenching is so low that the system should ideally remain in the ground state of the initial Hamiltonian and should have no current. However, the finiteness of τ leads to some excited states, which give a finite contribution to the current (represented by the dashed horizontal line). (b) A linear slow quench (i.e., τ large) from the trivial phase to the topological. The system maintains the instantaneous ground state of the time-evolved Hamiltonian, at each instant of time, and postquench it reaches the actual ground-state current of the final Hamiltonian (represented by the dashed horizontal line). (See also the sudden quench case of Cao *et al.* [51,52].)

IV. EDGE CURRENT DYNAMICS FOLLOWING A FINITE-TIME LINEAR QUENCH PROTOCOL

Following the brief discussion of the sudden and the adiabatic quench cases, we now turn our attention to the more interesting case of the dynamics during the intermediate times between the extreme sudden and the slow limits. To be specific, we drive the system from the nontopological ($M = 6$) to the topological ($M = 0$) phase keeping $\phi = \pi/3$ fixed, with different τ values (varying from 0.0001 to 500) and calculate the current at the N th edge for $t_f = \tau$, just as the quenching stops. Naively we can expect the ramp-up of the edge current from 0 for $\tau \rightarrow 0$ to the final equilibrium value for $\tau \gg L^2$ to be monotonic. However, it turns out that this is not

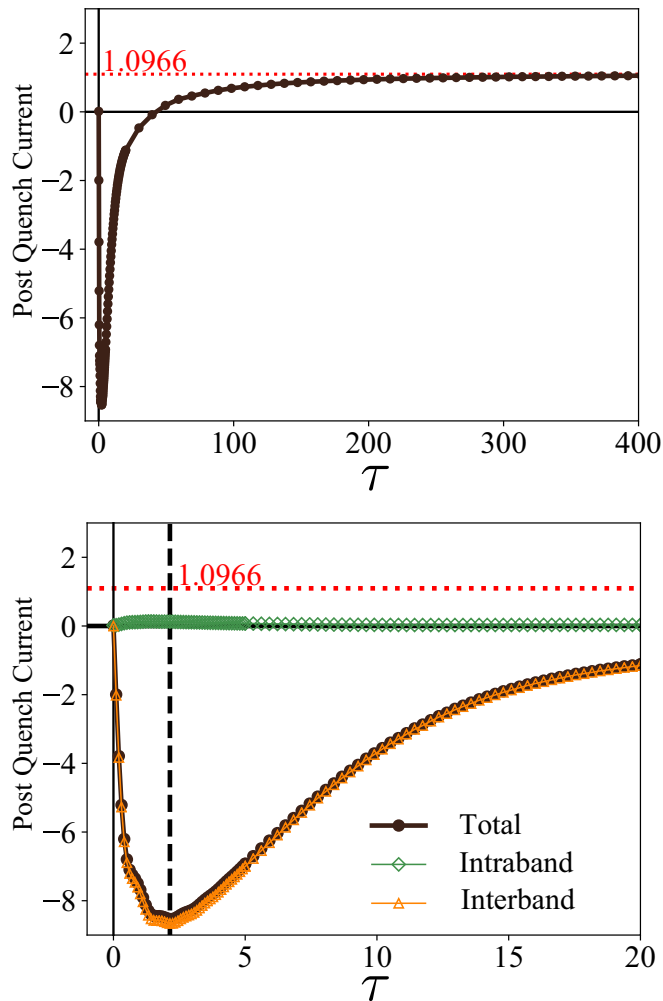


FIG. 6. (a) Variation of the postquench current for a linear sweep from a nontopological to a topological phase at different quenching rates τ . Here $\phi = \pi/3$, $t_1 = 1$, and $t_2 = 1/3$ are held fixed, while the Semenoff mass M is varied concerning the time to quench to different phases. The curve (represented by the solid line with filled circles) shows a generation of excess current for smaller values of τ which reaches a minimum at $\tau_0 = 2.2$ (represented by the dashed vertical line), following which it increases again to reach the equilibrium current value of the final Hamiltonian (represented by the dotted horizontal line) for large τ . (b) Zoomed-in version of the $\tau \in (0, 20)$ region of (a), with the intraband (solid line with diamonds) and interband (solid line with triangles) contributions [see Eq. (6)] shown separately. Clearly the excited states play a significant role, since the current is dominated by the interband contribution.

the case. Interestingly, the current is in the opposite direction than is usually expected.

The variation of the postquench current as a function of τ is shown in Fig. 6(a). To start with in the topologically trivial phase, for $\tau = 0$ the current is 0 as expected. On the other hand, for $\tau = 400 (\approx L^2)$, with $L = 20$, i.e., in the slow quench regime, the system always follows the instantaneous ground state of the time-evolved Hamiltonian and eventually reaches the ground state of the topological phase with $M = 0$ and $\phi = \pi/3$. Thus the edge current (calculated at $t = \tau$) also reaches its equilibrium value in the topological phase, for large

$\tau \sim L^2$. Interestingly, the evolution of the edge current with τ is not monotonic. Starting from zero edge current in the sudden quench regime, the edge current first decreases until a crossover value of $\tau = \tau_0$ and then increases again with increasing τ , to finally reach its adiabatic limit equilibrium value. For the particular linear quench protocol with $M_i = 6$, $M_f = 0$, $\phi = \pi/3$ shown in Figs. 6(a) and 6(b), we find that $\tau_0 = 2.2$. Remarkably, the absolute value of the current at $\tau = \tau_0$ is significantly larger than the absolute value of the edge current as $\tau \rightarrow \infty$.

The current operator can also be written as the sum of two parts, the interband and intraband currents, in terms of the eigenstates of the initial Hamiltonian. We have $\langle J_n^x \rangle = \sum_r \langle J_n^x \rangle_r$, where r simply denotes the index of the occupied bands, and

$$\begin{aligned}
 \langle \hat{J}_n^x \rangle_r &= \sum_{k_x} \langle \psi_r^{k_x}(0) | U_{k_x}^\dagger(t) \hat{J}_{n,k_x}^x U_{k_x}(t) | \psi_r^{k_x}(0) \rangle \\
 &= \sum_p \sum_{k_x} \langle \psi_r^{k_x}(t) | e_p^{k_x} \rangle \langle e_p^{k_x} | \hat{J}_{n,k_x}^x | e_p^{k_x} \rangle \langle e_p^{k_x} | \psi_r^{k_x}(t) \rangle \\
 &\quad + \sum_{p,q \neq p} \sum_{k_x} \langle \psi_r^{k_x}(t) | e_p^{k_x} \rangle \langle e_p^{k_x} | \hat{J}_{n,k_x}^x | e_q^{k_x} \rangle \langle e_q^{k_x} | \psi_r^{k_x}(t) \rangle \\
 &= \sum_{p=q} \sum_{k_x} |\langle \psi_r^{k_x}(t) | e_p^{k_x} \rangle|^2 \langle \hat{J}_{n,k_x}^x \rangle_p^{\text{intra}} \\
 &\quad + \sum_{p,q \neq p} \sum_{k_x} \langle \psi_r^{k_x}(t) | e_p^{k_x} \rangle \langle e_q^{k_x} | \psi_r^{k_x}(t) \rangle \langle \hat{J}_{n,k_x}^x \rangle_{pq}^{\text{inter}} \quad (6)
 \end{aligned}$$

Here, $|e_p\rangle$ and $|e_q\rangle$ are the eigenstates of the initial Hamiltonian, p and q are the band indices, and two parts of Eq. (6) represent the intraband and interband contributions to the total current, respectively. As shown in Fig. 6(b), the dominant contribution to the edge current comes from the interband contribution, with the intraband contribution being relatively small.

Edge current reversal

To understand the reversal in the direction of the edge current, as opposed to a monotonic rise from 0 with increasing τ , let us focus on the small-time behavior of the time evolution operator: $i\partial_t U(t) = H(t)U(t)$. For an infinitesimal increment of $\delta t/2$ in time, we have

$$U\left(\frac{\delta t}{2}\right) = U(0) - iH(0)U(0)\frac{\delta t}{2}. \quad (7)$$

Propagating to another increment of $\delta t/2$ interval,

$$U(\delta t) = U\left(\frac{\delta t}{2}\right) - iH\left(\frac{\delta t}{2}\right)U\left(\frac{\delta t}{2}\right)\frac{\delta t}{2}. \quad (8)$$

Since we are looking at the small- τ limit in the vicinity of the sudden quench, we set $\tau = \delta t$ —the point at which the final current has to be calculated. Thus we have

$$H\left(\frac{\delta t}{2}\right) = H(0) + V\left(\frac{\delta t}{2}\right), \quad (9)$$

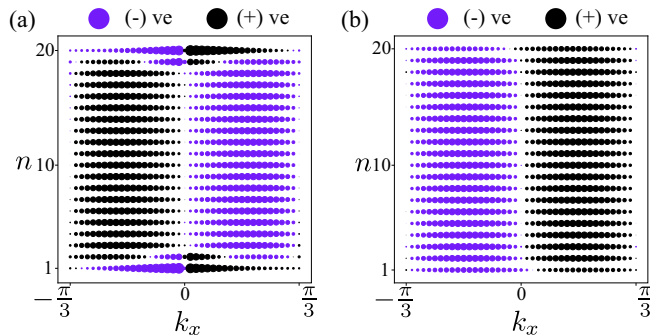


FIG. 7. Spatial n (see Fig. 2) and k_x -resolved current in (a) the topological phase and (b) the nontopological phase. The size of the circle represents the amount of current at that point and the color denotes the sign of the current (blue-violet, negative; black, positive). The existence of a finite edge current in the topological phase (a) and no current in the nontopological phase (b) is evident.

with $H(0) = H(M_i)$, and

$$V\left(\frac{\delta t}{2}\right) = \frac{(M_i - M_f) \delta t}{\tau} \Sigma_z, \quad (10)$$

where we have defined

$$\Sigma_z = \begin{pmatrix} 1 & 0 & 0 & 0 & \cdots \\ 0 & -1 & 0 & 0 & \cdots \\ 0 & 0 & 1 & 0 & \cdots \\ 0 & 0 & 0 & -1 & \cdots \\ \vdots & \vdots & \vdots & \vdots & \ddots \end{pmatrix}. \quad (11)$$

Using Eq. (7) and Eq. (9) in Eq. (8) and restricting up to linear order in δt (neglecting higher order terms, which may render it nonunitary), a simplified form of the unitary operator can be obtained, and it is given by

$$U(\delta t) = \mathbb{1} - i \left[H(M_i) - \frac{M_i - M_f}{4} \Sigma_z \right] \delta t. \quad (12)$$

Now, the time-evolved state under this unitary operator is given by

$$|\psi_{p,k}(\delta t)\rangle = U(\delta t) |\psi_{p,k}(0)\rangle, \quad (13)$$

where p denotes the band index and $k = k_x$. Finally, the expectation value of the edge current, to lowest order in δt , is given by

$$\begin{aligned} J^x(\delta t) &= \sum_{p,k} \langle \psi_{p,k}(\delta t) | \hat{J}_k^x | \psi_{p,k}(\delta t) \rangle \\ &= \sum_{p,k} \langle \psi_{p,k}(0) | \hat{J}_k^x | \psi_{p,k}(0) \rangle + i \left(\frac{M_i - M_f}{4} \right) \delta t \\ &\quad \times \sum_{p,k} \langle \psi_{p,k}(0) | [\hat{J}_k^x, \Sigma_z] | \psi_{p,k}(0) \rangle. \end{aligned} \quad (14)$$

Here the first term is simply the initial equilibrium current, which is 0 for a starting point in the nontopological phase. In Eq. (14), the second term brings in the effect of the time evolution for small $\delta t = \tau$.

To understand the small-time limit better, we show the spatially resolved current in the final topological phase, and

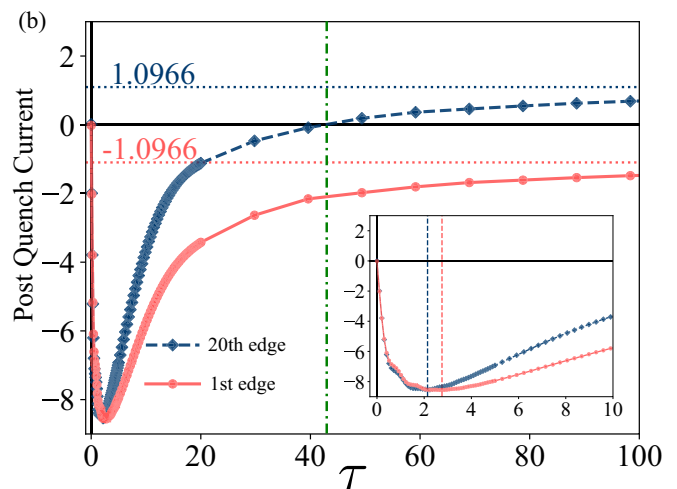
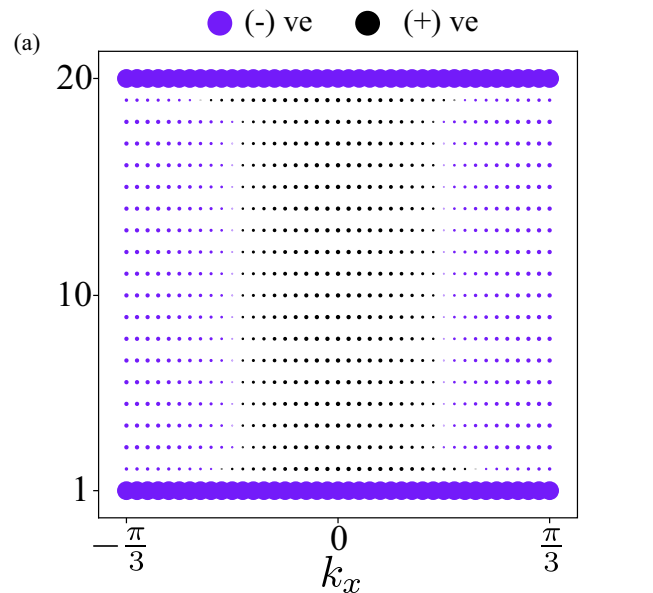


FIG. 8. (a) Spatial n and k_x -resolved contribution to the edge current of the dynamical part [arising from the second term in Eq. (14)] for small τ values. (b) The unidirectional negative contribution in both edges leads to the huge initial dip in current at both edges. The size of the circle in (a) is proportional to the magnitude of the current. Here all the parameters are identical to those in Fig. 6. (b) Variation of the postquench current (calculated at $t = \tau$) at different quenching rates τ at the two edges of the system (represented by the dashed line with diamonds and the solid line with circles). Starting from the $\tau = 0$ scenario of zero current, the current eventually goes to the respective equilibrium value (represented by dotted horizontal lines) for both edges at large τ , though for small τ both edges show a large dip in current and have different values of the turning point τ_0 (highlighted in the inset). The dot-dashed vertical line indicates the value of τ after which the current at the two edges propagates in opposite directions.

the initial trivial phase in Figs. 7(a) and 7(b), respectively. Evidently in Fig. 7(a), there is only an edge current propagating in opposite directions on the two edges in the topological phase, while there is absolutely no current to start with in the no-topological phase. The impact of the second term in Eq. (14), is shown in Fig. 8(a). Clearly the second term in Eq. (14) forces a large unidirectional negative current in both

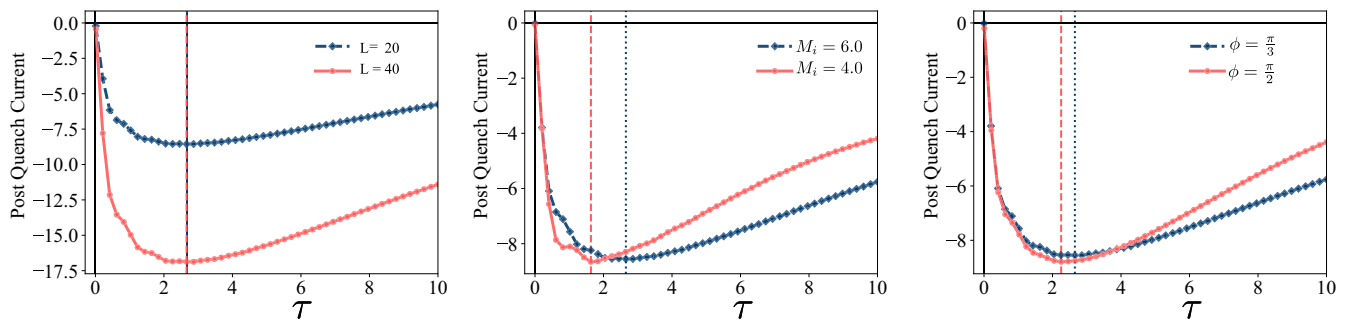


FIG. 9. Dependence of τ_0 (for a given edge) on various system parameters. (a) τ_0 is independent of the width of the Haldane nanoribbon. However, τ_0 seems to depend on the parameters which determine the topological phase of the system, i.e., on (b) the Semenoff mass M and (c) the Haldane flux ϕ . The positions of τ_0 for different parameters are represented by vertical lines.

edges of the Haldane nanoribbon at very small τ . This leads to nonmonotonic behavior of the τ -dependent current, since the large negative current in both edges of the Haldane nanoribbon generated for very small τ has to eventually relax to the respective equilibrium values (equal in magnitude and opposite in direction) for both edges at large τ , as shown in Fig. 8(b). τ_0 , however, is not the same for the two edges in general [see Fig. 8(b), inset]. It depends on both the Semenoff mass terms M_i/M_f and the value of ϕ . Thus, its location on the τ axis completely depends on such nonuniversal features, and hence, the different τ_0 's for the two boundaries can even be separately tuned to coincide. The behavior of the edge currents at the two edges in the nonequilibrium scenario can only be analytically ascertained for the limits of $\tau \rightarrow 0$ and $\tau \rightarrow \infty$; the value of τ_0 at which the edge current dips to assume a minimum value is an early τ behavior which, being nonuniversal, can only be determined numerically. It should also be understood that these are not finite-size effects, as τ_0 is independent of the linear dimensions of the system under consideration as illustrated in Fig. 9(a).

One of the most interesting facts is that there is a finite value of $\tau = \tau_a$ [approximately $\tau_a \simeq 42$ in Fig. 8(b)] such that for $\tau < \tau_a$ the current in both edges is in the same direction, and precisely at $\tau = \tau_a$, the current in one of the edges (that carries a positive current in the equilibrium situation) vanishes. This may imply a “dynamical localization” of the current generated for $t < \tau_a$ during the ramping. We call this a dynamical localization because the vanishing of the edge current at a certain τ is an artifact of dynamics which has *no* equilibrium counterpart. This is in complete contrast with the conventional single-particle Anderson localization observed in real space in the presence of disorder. Note that for a given set of initial Semenoff masses in the nontopological phase and the final Semenoff masses in the topological phase, we always find a set of τ 's for which the edge current vanishes for one edge of our model given our choice of driving protocol. Even though the topological edges cannot be localized in a conventional sense, the vanishing of edge current observed in these situations points to an emergent dynamical localization. On the contrary, when τ exceeds τ_a , the edge current reverses sign for one of the edges, implying that the adiabatic effect starts dominating at $\tau > \tau_a$. While the origin of the nonmonotonic behavior of the edge current in the Haldane nanoribbon is now clear, the nature of τ_0 and its dependence on various system parameters are still

unknown. It turns out that τ_0 does not depend on the system size at all [see Fig. 9(a)] and is sensitive only to changes in the parameters deciding the topology of the phase, i.e., M [see Fig. 9(b)] and ϕ [see Fig. 9(c)]. We would like to mention that the parameter t_2 is defined with respect to t_1 which is in turn set to unity throughout our work. The topological phase diagram of the Haldane model is usually plotted in the (M/t_2) - ϕ plane as shown in Fig. 1(d). Hence, we believe that analyzing the variation of τ_0 with the ratio M/t_2 (with $t_2 = 1/3$) and the parameter ϕ would be sufficient. Although we observed that the value of τ_0 at large M_i is larger than its value at small M_i (with M_f fixed), deciphering its behavior is quite complicated and nontrivial. Furthermore, the behavior of τ_0 with ϕ is definitely nonlinear and nonmonotonic and is immensely difficult to investigate under the current scope of this work.

We also note that there are fine structures in the form of kinks in the plots for the postquench current as a function of τ [see Fig. 9(b), for example]. These kinks or oscillations in the transients in current are early time effects (i.e., small τ) and are present for each k mode. When the contributions for each mode are summed up, there are coherent superpositions that result in such a structure. Such coherent superpositions die off with increasing τ . These kinks are nonuniversal in the sense that they depend on the quenching parameters involved. The early time transients can be understood to originate from Rabi oscillations between the levels of the N -level system, and thereby they qualitatively depend on the band gaps between levels and the driving frequencies and amplitude involved.

V. CONCLUSION

To summarize, we have investigated the nonequilibrium dynamics of the edge current of the semiopen Haldane model, subjected to a time-dependent linear quench from the nontopological phase to the topological phase. In the sudden quench limit, the system retains its original ground state even for a quench across the phase boundary, and consequently the edge current just retains its initial value dictated by the starting phase. When the starting point is in the nontopological phase, the edge current remains 0 at all times for a sudden quench. In the opposite limit of slow quench (adiabatic limit), at each moment the system relaxes to the instantaneous ground state of the time-dependent Hamiltonian throughout the quenching

path, yielding a final edge current dictated only by the ground-state current of the final Hamiltonian.

Interestingly, we find that with increasing τ , the change in the current from the initial phase current for $\tau \rightarrow 0$ to the final phase current for $\tau \rightarrow \infty$ is not monotonic. In the small- τ limit, there is a large unidirectional current generated on both edges of the Haldane nanoribbon. This causes the initial current to change drastically, and then with increasing τ the currents at both edges relax to their final equilibrium values, which are equal in magnitude but opposite in direction. This leads to a nonmonotonic behavior of the edge current with τ . We find that the turning point for the nonmonotonic edge current, τ_0 , is different for the two edges, does not depend on the system size, and is sensitive only to the Semenoff mass M and the Haldane flux ϕ . Furthermore, we also establish the existence of another time scale τ_a such that, for $\tau > \tau_a$, the adiabatic effect starts to dominate.

Finally, we note that in this work, the finite geometry of the Haldane model has been realized on a graphene lattice with armchair edges. Indeed there is also a possibility of realizing the same for the other case, namely, the zigzag boundary. A detailed study on topological edge states for the two different edges of the Haldane model has been carried out by Hao *et al.* [64]. It is apparent from their work that the phase diagram of this system, which is determined by the bulk Chern number, predicts the existence of edge states in a semiopen system, for both the armchair and the zigzag boundaries. Since both armchair and zigzag edges have similar edge properties, we expect the zigzag boundary to exhibit the same dynamics of the edge current as well. While most of our discussion is specifically for the Haldane model on a nanoribbon, we expect similar physics to play out in other systems with topological phases and the associated edge state.

ACKNOWLEDGMENT

A.D. acknowledges SERB, DST, New Delhi for financial support.

APPENDIX: NUMERICAL METHODS

In this Appendix, we briefly discuss the numerical techniques involved in calculating the edge currents at the two boundaries of the sample with armchair edges. The system under study, being periodically wrapped along the x direction, yields the quasimomentum k_x as a good quantum number. This allows us to choose a finitely large unit cell along the y direction as shown in Fig. 2 which includes sites (y) labeled with the site numbers from 1 to N and sublattice indices $s = A, B$. Thus, in the basis of $|y, s\rangle = |y\rangle \odot |s\rangle$, in accordance with Eq. (4), we can write the Hamiltonian as a $2N \times 2N$ matrix parametrized by each conserved quasimomentum mode k_x . Since the diagonal elements of this Hamiltonian contain the Semenoff mass term, $M(t) = M_i + (M_f - M_i)t/\tau$ (defined within $0 \leq t \leq \tau$), which are globally time dependent, one now needs to solve the time-dependent Schrodinger equation:

$$i \frac{\partial \psi_{2N \times 1}(t)}{\partial t} = H_{2N \times 2N}(t) \psi_{2N \times 1}(t). \quad (\text{A1})$$

Here, $|\psi(t)\rangle = \sum_{y=1, s=A, B}^N c_{y,s}(t) |y, s\rangle$ gives the column vector,

$$\psi_{2N \times 1}(t) = (c_{1,A} \quad c_{1,B} \dots c_{y,A} \quad c_{y,B} \dots c_{N,A} \quad c_{N,B})^T, \quad (\text{A2})$$

and $H_{2N \times 2N}(t)$ is a time-dependent matrix. Now using the initial ground state $\psi_{2N \times 1}(0)$ of $H_{2N \times 2N}(t=0)$ as the boundary condition, we solve these $2N$ sets of coupled linear differential equations, from initial time $t_i = 0$ to final time $t_f = \tau$, numerically. We use the ODEINT package in Python to obtain the time-dependent state vector $\psi_{2N \times 1}(t=t_f=\tau)$ of the system, using a suitable time step to ensure numerical accuracy. Finally, the expressions of the edge currents at any edge of the system $y = 1$ or N can be obtained by utilizing Eq. (5) and writing it in the form of an extremely sparse $2N \times 2N$ matrix in the same basis ($|y, s\rangle$) as the Hamiltonian matrix and taking its expectation value with respect to the $\psi_{2N \times 1}(\tau)$ of the system evaluated above.

-
- [1] B. K. Stuhl, H.-I. Lu, L. M. Ayccock, D. Genkina, and I. B. Spielman, Visualizing edge states with an atomic bose gas in the quantum hall regime, *Science* **349**, 1514 (2015).
- [2] G. Jotzu, M. Messer, R. Desbuquois, M. Lebrat, T. Uehlinger, D. Greif, and T. Esslinger, Experimental realization of the topological Haldane model with ultracold fermions, *Nature* **515**, 237 (2014).
- [3] M. Atala, M. Aidelsburger, J. T. Barreiro, D. Abanin, T. Kitagawa, E. Demler, and I. Bloch, Direct measurement of the Zak phase in topological Bloch bands, *Nat. Phys.* **9**, 795 (2013).
- [4] M. Killi, S. Trotzky, and A. Paramekanti, Anisotropic quantum quench in the presence of frustration or background gauge fields: A probe of bulk currents and topological chiral edge modes, *Phys. Rev. A* **86**, 063632 (2012).
- [5] P. Hauke, M. Lewenstein, and A. Eckardt, Tomography of Band Insulators from Quench Dynamics, *Phys. Rev. Lett.* **113**, 045303 (2014).
- [6] A. G. Grushin, S. Roy, and M. Haque, Response of fermions in Chern bands to spatially local quenches, *J. Stat. Mech.: Theory Exp.* (2016) 083103.
- [7] M. Greiner, O. Mandel, T. W. Hänsch, and I. Bloch, Collapse and revival of the matter wave field of a Bose–Einstein condensate, *Nature* **419**, 51 (2002).
- [8] T. Oka and H. Aoki, Photovoltaic Hall effect in graphene, *Phys. Rev. B* **79**, 081406 (2009).
- [9] T. Kitagawa, T. Oka, A. Brataas, L. Fu, and E. Demler, Transport properties of nonequilibrium systems under the application of light: Photoinduced quantum Hall insulators without Landau levels, *Phys. Rev. B* **84**, 235108 (2011).
- [10] M. S. Rudner, N. H. Lindner, E. Berg, and M. Levin, Anomalous edge states and the bulk-edge correspondence for periodically driven two-dimensional systems, *Phys. Rev. X* **3**, 031005 (2013).

- [11] L. E. F. Foa Torres, P. M. Perez-Piskunow, C. A. Balseiro, and G. Usaj, Multiterminal Conductance of a Floquet Topological Insulator, *Phys. Rev. Lett.* **113**, 266801 (2014).
- [12] H. Dehghani, T. Oka, and A. Mitra, Out-of-equilibrium electrons and the Hall conductance of a Floquet topological insulator, *Phys. Rev. B* **91**, 155422 (2015).
- [13] J. H. Wilson, J. C. W. Song, and G. Refael, Remnant Geometric Hall Response in a Quantum Quench, *Phys. Rev. Lett.* **117**, 235302 (2016).
- [14] S. Sharma, V. Mukherjee, and A. Dutta, Study of Loschmidt echo for a qubit coupled to an xy-spin chain environment, *Eur. Phys. J. B* **85**, 143 (2012).
- [15] M. Heyl, A. Polkovnikov, and S. Kehrein, Dynamical Quantum Phase Transitions in the Transverse-Field Ising Model, *Phys. Rev. Lett.* **110**, 135704 (2013).
- [16] C. Karrasch and D. Schuricht, Dynamical phase transitions after quenches in nonintegrable models, *Phys. Rev. B* **87**, 195104 (2013).
- [17] J. C. Budich and M. Heyl, Dynamical topological order parameters far from equilibrium, *Phys. Rev. B* **93**, 085416 (2016).
- [18] U. Bhattacharya and A. Dutta, Emergent topology and dynamical quantum phase transitions in two-dimensional closed quantum systems, *Phys. Rev. B* **96**, 014302 (2017).
- [19] M. Heyl, Scaling and Universality at Dynamical Quantum Phase Transitions, *Phys. Rev. Lett.* **115**, 140602 (2015).
- [20] T. Palmari, Edge exponents in work statistics out of equilibrium and dynamical phase transitions from scattering theory in one-dimensional gapped systems, *Phys. Rev. B* **92**, 235433 (2015).
- [21] S. Vajna and B. Dóra, Disentangling dynamical phase transitions from equilibrium phase transitions, *Phys. Rev. B* **89**, 161105 (2014).
- [22] S. Sharma, S. Suzuki, and A. Dutta, Quenches and dynamical phase transitions in a nonintegrable quantum Ising model, *Phys. Rev. B* **92**, 104306 (2015).
- [23] S. Vajna and B. Dóra, Topological classification of dynamical phase transitions, *Phys. Rev. B* **91**, 155127 (2015).
- [24] M. Schmitt and S. Kehrein, Dynamical quantum phase transitions in the Kitaev honeycomb model, *Phys. Rev. B* **92**, 075114 (2015).
- [25] S. Sharma, U. Divakaran, A. Polkovnikov, and A. Dutta, Slow quenches in a quantum Ising chain: Dynamical phase transitions and topology, *Phys. Rev. B* **93**, 144306 (2016).
- [26] U. Divakaran, S. Sharma, and A. Dutta, Tuning the presence of dynamical phase transitions in a generalized xy spin chain, *Phys. Rev. E* **93**, 052133 (2016).
- [27] U. Bhattacharya and A. Dutta, Interconnections between equilibrium topology and dynamical quantum phase transitions in a linearly ramped Haldane model, *Phys. Rev. B* **95**, 184307 (2017).
- [28] A. Dutta and A. Dutta, Probing the role of long-range interactions in the dynamics of a long-range Kitaev chain, *Phys. Rev. B* **96**, 125113 (2017).
- [29] V. Mukherjee, S. Sharma, and A. Dutta, Loschmidt echo with a nonequilibrium initial state: Early-time scaling and enhanced decoherence, *Phys. Rev. B* **86**, 020301 (2012).
- [30] S. Suzuki, T. Nag, and A. Dutta, Dynamics of decoherence: Universal scaling of the decoherence factor, *Phys. Rev. A* **93**, 012112 (2016).
- [31] B. Dóra, F. Pollmann, J. Fortágh, and G. Zaránd, Loschmidt Echo and the Many-Body Orthogonality Catastrophe In a Qubit-Coupled Luttinger Liquid, *Phys. Rev. Lett.* **111**, 046402 (2013).
- [32] R. Sachdeva, T. Nag, A. Agarwal, and A. Dutta, Finite-time interaction quench in a Luttinger liquid, *Phys. Rev. B* **90**, 045421 (2014).
- [33] U. Bhattacharya, S. Bandyopadhyay, and A. Dutta, Mixed state dynamical quantum phase transitions, *Phys. Rev. B* **96**, 180303 (2017).
- [34] M. Thakurathi, A. A. Patel, D. Sen, and A. Dutta, Floquet generation of majorana end modes and topological invariants, *Phys. Rev. B* **88**, 155133 (2013).
- [35] M. Thakurathi, K. Sengupta, and D. Sen, Majorana edge modes in the Kitaev model, *Phys. Rev. B* **89**, 235434 (2014).
- [36] V. Mukherjee and A. Dutta, Effects of interference in the dynamics of a spin-1/2 transverse xy chain driven periodically through quantum critical points, *J. Stat. Mech.: Theory Exp.* (2009) P05005.
- [37] A. Das, Exotic freezing of response in a quantum many-body system, *Phys. Rev. B* **82**, 172402 (2010).
- [38] H. T. Quan, Z. Song, X. F. Liu, P. Zanardi, and C. P. Sun, Decay of Loschmidt Echo Enhanced by Quantum Criticality, *Phys. Rev. Lett.* **96**, 140604 (2006).
- [39] T. Nag, U. Divakaran, and A. Dutta, Scaling of the decoherence factor of a qubit coupled to a spin chain driven across quantum critical points, *Phys. Rev. B* **86**, 020401 (2012).
- [40] S. Sharma, A. Russomanno, G. E. Santoro, and A. Dutta, Loschmidt echo and dynamical fidelity in periodically driven quantum systems, *Europhys. Lett.* **106**, 67003 (2014).
- [41] T. Nag, S. Roy, A. Dutta, and D. Sen, Dynamical localization in a chain of hard core bosons under periodic driving, *Phys. Rev. B* **89**, 165425 (2014).
- [42] A. Agarwala, U. Bhattacharya, A. Dutta, and D. Sen, Effects of periodic kicking on dispersion and wave packet dynamics in graphene, *Phys. Rev. B* **93**, 174301 (2016).
- [43] A. Lazarides, A. Das, and R. Moessner, Fate of Many-Body Localization Under Periodic Driving, *Phys. Rev. Lett.* **115**, 030402 (2015).
- [44] U. Bhattacharya, S. Dasgupta, and A. Dutta, Dynamical merging of Dirac points in the periodically driven Kitaev honeycomb model, *Eur. Phys. J. B* **89**, 216 (2016).
- [45] S. Dasgupta, U. Bhattacharya, and A. Dutta, Phase transition in the periodically pulsed Dicke model, *Phys. Rev. E* **91**, 052129 (2015).
- [46] U. Bhattacharya, S. Maity, U. Banik, and A. Dutta, Exact results in Floquet coin toss for driven integrable models, [arXiv:1705.03662](https://arxiv.org/abs/1705.03662) [cond-mat.stat-mech].
- [47] G.-W. Chern, C.-C. Chien, and M. Di Ventra, Dynamically generated flat-band phases in optical kagome lattices, *Phys. Rev. A* **90**, 013609 (2014).
- [48] C. Wang, P. Zhang, X. Chen, J. Yu, and H. Zhai, Scheme to Measure the Topological Number of a Chern Insulator from Quench Dynamics, *Phys. Rev. Lett.* **118**, 185701 (2017).
- [49] M. Tarnowski, F. Nur Ünal, N. Fläschner, B. S. Rem, A. Eckardt, K. Sengstock, and C. Weitenberg, Characterizing topology by dynamics: Chern number from linking number, [arXiv:1709.01046](https://arxiv.org/abs/1709.01046) [cond-mat.quant-gas].
- [50] F. D. M. Haldane, Model for a Quantum Hall Effect Without Landau Levels: Condensed-Matter Realization of the “Parity Anomaly”, *Phys. Rev. Lett.* **61**, 2015 (1988).

- [51] M. D. Caio, N. R. Cooper, and M. J. Bhaseen, Quantum Quenches in Chern Insulators, *Phys. Rev. Lett.* **115**, 236403 (2015).
- [52] M. D. Caio, N. R. Cooper, and M. J. Bhaseen, Hall response and edge current dynamics in Chern insulators out of equilibrium, *Phys. Rev. B* **94**, 155104 (2016).
- [53] L. D'Alessio and M. Rigol, Dynamical preparation of Floquet Chern insulators, *Nat. Commun.* **6**, 8336 (2015).
- [54] D. Sticlet and F. Piéchon, Distant-neighbor hopping in graphene and Haldane models, *Phys. Rev. B* **87**, 115402 (2013).
- [55] U. Bhattacharya, J. Hutchinson, and A. Dutta, Quenching in Chern insulators with satellite Dirac points: The fate of edge states, *Phys. Rev. B* **95**, 144304 (2017).
- [56] M. S. Foster, V. Gurarie, M. Dzero, and E. A. Yuzbashyan, Quench-Induced Floquet Topological p -Wave Superfluids, *Phys. Rev. Lett.* **113**, 076403 (2014).
- [57] M. S. Foster, M. Dzero, V. Gurarie, and E. A. Yuzbashyan, Quantum quench in a $p + ip$ superfluid: Winding numbers and topological states far from equilibrium, *Phys. Rev. B* **88**, 104511 (2013).
- [58] G. W. Semenoff, Condensed-Matter Simulation of a Three-Dimensional Anomaly, *Phys. Rev. Lett.* **53**, 2449 (1984).
- [59] L. D. Landau, Zur theorie der energieübertragung. II, *Phys. Z. Sowjetunion* **2**, 1 (1932).
- [60] C. Zener, Non-adiabatic crossing of energy levels, *Proc. R. Soc. London A* **137**, 696 (1932).
- [61] A. V. Shytov, Landau-Zener transitions in a multilevel system: An exact result, *Phys. Rev. A* **70**, 052708 (2004).
- [62] N. V. Vitanov and B. M. Garraway, Landau-Zener model: Effects of finite coupling duration, *Phys. Rev. A* **53**, 4288 (1996).
- [63] N. V. Vitanov, Transition times in the Landau-Zener model, *Phys. Rev. A* **59**, 988 (1999).
- [64] N. Hao, P. Zhang, Z. Wang, W. Zhang, and Y. Wang, Topological edge states and quantum Hall effect in the Haldane model, *Phys. Rev. B* **78**, 075438 (2008).